nature photonics

Article

https://doi.org/10.1038/s41566-026-01898-z

Wide-band millimetre-wave synthesizer using microresonator-soliton photomixing

Received: 12 December 2025

Accepted: 23 March 2026

Published online: 05 May 2026

Check for updates

Jizhao Zang[1,2] ✉, Travis C. Briles[1], Jesse S. Morgan[3], Andreas Beling[3] & Scott B. Papp[1,2] ✉

Millimetre-wave and terahertz signals enable high-performance applications; however, tunable integrated electronics remain limited beyond 100 GHz, restricting progress in wireless communication, high-resolution imaging, and spectroscopy. Photonic approaches can address this, albeit with increased size and power consumption. Here we describe a chip-scale, wide-band millimetre-wave frequency synthesizer, which uses integrated nonlinear photonics and high-speed photodetection to exploit the nearly limitless bandwidth of light. We generate dual, microresonator-soliton frequency combs whose interferogram is fundamentally composed of harmonic signals spanning the millimetre-wave and terahertz bands. By phase coherence of the dual comb, we precisely stabilize the interferogram to generate any output frequency from direct current to >1 THz. Across this range, the synthesizer exhibits exceptional frequency stability, characterized by an Allan deviation of 3×10^{-12} in 1-s measurements; and low phase noise, achieving −83 dBc Hz^{-1} at 100 kHz offset and a reference frequency of 150 GHz. We use a modified uni-travelling-carrier photodiode with an operating frequency up to 500 GHz to convert the interferogram to an electrical signal, with continuously tunable tones. Our work harnesses the coherence, bandwidth and integration of photonics to extend the accessible frequency range of current, advanced-node complementary metal–oxide–semiconductor microwave electronics to the millimetre-wave and terahertz bands.

Phase-stable frequency synthesis is a principal technology for universally important applications in communication, information processing, ranging, positioning, timing and sensing[1–5]. Digital electronics enable fully phase-coherent signal generation and detection across the microwave band, supporting, for example, the high-speed data streams at the core of mobile devices with increasingly rich functionalities. However, the growing demand for information capacity in wired and wireless networks[6] and emerging sensing approaches with high resolution[7,8] highlight the need for access to higher-frequency bands, which are generally more challenging to implement with digital electronics.

The millimetre-wave (mmW) and terahertz (THz) bands extend from 30 to 300 GHz and to tens of THz, respectively. Beyond increased bandwidth, resolution and speed for applications, mmW and THz bands offer unique opportunities to characterize materials[9,10]. Hence, there is a long history of developing mmW and THz sources, including free-electron vacuum devices[11], solid-state diodes[12,13], quantum cascade lasers[14] and integrated electronic circuits[15]. By building on miniaturized voltage-controlled oscillators (VCOs), phase-locked loops (PLLs), electronic filters, frequency multipliers and other silicon microelectronic components, digital complementary

[1]Time and Frequency Division, National Institute of Standards and Technology, Boulder, CO, USA. [2]Department of Physics, University of Colorado, Boulder, CO, USA. [3]Department of Electrical and Computer Engineering, University of Virginia, Charlottesville, VA, USA. ✉e-mail: jz4nd@virginia.edu; scott.papp@nist.gov

metal–oxide–semiconductor (CMOS) frequency synthesizers[15–19] define the state-of-the-art for widespread applications in the mmW and THz bands, including signal analysis, radar sensing and high-speed communications. However, the phase noise of electronic synthesizers is fundamentally limited by frequency division and multiplication.

Photonic techniques for mmW synthesis generally involve laser sources that are heterodyne-detected to generate an electronic signal. Numerous photonic technologies have been reported to implement mmW synthesizers, including frequency multiplexing with electro-optic (EO) modulators[20], mixing two lasers locked to optical frequency combs[21,22], and Brillouin lasers using fibre cavity or disk resonators[23,24]. Approaches that rely solely on modulators are challenging or impossible to scale to high-frequency signals owing to the low power of high-order modulation sidebands. Injection locking has been introduced to increase the power of high-order sidebands for mmW generation, but continuous frequency tuning requires precise alignment between the sidebands and laser free-running frequency due to the narrow locking range of distributed feedback lasers under weak injection[25]. mmW generation using fibre frequency combs provides a wide frequency-tuning range, but such systems cannot be integrated, and they suffer from the low efficiency of the comb source. Synthesizers based on Brillouin lasers offer high frequency stability, but their frequency tuning range is narrow. Until now, a compact frequency synthesizer with tuning across the mmW and THz bands has not been demonstrated.

The recent development of Kerr-microresonator solitons[26–31] has provided a promising laser source to realize chip-scale electronic frequency synthesizers. Such soliton microcombs intrinsically operate with repetition frequencies in the microwave and mmW bands, and their photodetection produces a low-phase-noise electronic signal[32–34]. Building on developments in Tb/s optical data links, microcombs can provide high output power and high conversion efficiency[35–37]. Single microcomb schemes for electronic signal generation can offer high-performance spectral characteristics[38–42], but the frequency tuning range is narrow and the signal stability is still limited by the thermal noise[43] without locking to optical frequency references.

Here, we introduce a wideband electronic frequency synthesizer based on microresonator-soliton photomixing. The synthesizer is a photonic-integrated circuit with parallel-operating soliton microcombs and singular input and output ports for the pump laser and the dual microcomb, respectively. By heterodyne detection of the two soliton microcombs, we generate a set of highly coherent photocurrent tones that continuously span the microwave, mmW and even THz frequency ranges, which is distinct from the optical frequency synthesizer operating at 194 THz (ref. 4). Intensity modulation of the pump laser provides a frequency bias of the dual microcomb that continuously and completely tunes the synthesizer output. Indeed, we achieve mmW synthesis at 100 GHz, 150 GHz and up to 300 GHz, with an absolute fractional frequency accuracy of 3×10^{-12}, limited in our experiments by the reference clock and fibre delay noise. The phase noise of the synthesizer at 150 GHz is −83 dBc Hz^{-1} at 100-kHz offset, which outperforms the state-of-the-art frequency synthesizers in CMOS and SiGe BiCMOS electronics[16,17,19,44–46] (Supplementary Section 1). Leveraging the advantages of soliton microcombs such as photonic integration, low noise and low power consumption, our work demonstrates an architecture for a chip-scale frequency synthesizer that generates stable electrical signals from direct current (d.c.) to >1,000 GHz.

Results

Principle of the wide-band mmW frequency synthesizer

Figure 1 presents an overview of the electronic synthesizer, showing the concept of microresonator-soliton photomixing with integrated photonics and the synthesizer's exceptional frequency-tuning range. We highlight the key photonic elements of the synthesizer in Fig. 1a, including the dual-microresonator-soliton generator, the pump laser, the intensity modulator that creates two pump tones with a tunable frequency offset $\Delta\nu_p = 2f_{\mathrm{IM}}$, where f_{IM} is the modulation frequency for each microcomb, and the wavelength filtering and photodetection system that maps each mode pair of the dual microcomb to an electronic frequency. In our experiments, we explore different versions of the synthesizer with partial photonic integration (Fig. 1b) and with discrete microcomb chips, a bench laser system and fibre-integrated components. The key operational principle of the synthesizer is to use two soliton microcombs with a repetition-frequency difference of $\Delta\nu_{\mathrm{rep}}$ and a pump-frequency difference of $2f_{\mathrm{IM}}$, so that commensurate mode pairs of the microcombs exhibit an increasing and tunable frequency spacing $|\Delta\nu_{\mathrm{rep}} \pm 2f_{\mathrm{IM}}|$, $|2\Delta\nu_{\mathrm{rep}} \pm 2f_{\mathrm{IM}}|$, $|3\Delta\nu_{\mathrm{rep}} \pm 2f_{\mathrm{IM}}|$ and so on.

Fully integrating the synthesizer is an important goal. Our advance of partial integration—the dual-soliton microcomb system—highlights the potential for combination with other technologies (Fig. 1b). We have developed wafer-scale fabrication of soliton microcombs by several iterations of fabrication and testing with the Ligentec foundry[47]. For integration of the soliton system, we use a silicon nitride (Si_3N_4, hereafter SiN) waveguide layer with bottom and top SiO_2 claddings to implement the microcombs, which are joined to common chip-edge couplers with multimode interferometer (MMI) couplers. The ring resonance is tuned by the on-chip thermal heaters with a tuning rate of 0.52 nm V^{-1} at 1,550 nm. By optimizing the bias voltage applied to the heaters, we are able to align the ring resonances with the two pump tones, respectively.

To convert mode pairs of the dual-soliton microcomb to an electronic signal, we use a modified uni-travelling carrier (MUTC) photodiode[48–50] (Fig. 1c). By optimizing the photodiode design (Methods), we realize a photodiode with 3-dB bandwidth of 128 GHz (Supplementary Section 4), responsivity of 0.11 A W^{-1}, output power over −2.6 dBm at 160 GHz (ref. 49) and operational response to 500 GHz (ref. 50).

By tuning f_{IM}, we synthesize mmW signals with an extremely wide tuning range. Figure 1d presents optical-spectrum measurements of the synthesizer output with varying f_{IM}. We use two soliton microcombs with 1-THz and 950-GHz spacing, namely $\Delta\nu_{\mathrm{rep}}$ = 50 GHz, and tune f_{IM} around 25 GHz. The frequency spacing between the commensurate mode pairs is an integer multiple of 50 GHz such as 100 GHz, 150 GHz, 200 GHz and so on. The top inset is an enlarged view of the optical spectra, where we take the second mode pair in the lower-frequency side of the pump as an example. We generate mmW signals by separating the mode pairs with a wavelength-division multiplexer (WDM) and detecting them with the MUTC photodiode. For complete frequency tunability from d.c. to 300 GHz, the WDM should support six channels with a 3-dB bandwidth >300 GHz and a channel spacing of 975 GHz, which can be implemented using arrayed-waveguide grating structures[51] or multiplexer/demultiplexer systems based on Mach–Zehnder interferometers (MZIs) or cascaded ring resonators[52]. In the experiment, we use a tunable optical bandpass filter (OBPF) for simplicity. Figure 1e,f shows the electrical spectra of 150-GHz and 200-GHz mmW signals, respectively. At a photocurrent of 1.1 mA, we achieve an output power of −22 dBm for the 150-GHz mmW signal. We tune the mmW frequency across a range of 13 GHz with a step size of 1 GHz (Methods). In Fig. 1f, we observe a fast roll-off of power as frequency increases, which results from the increased insertion loss of the radio frequency (RF) components at frequencies beyond its nominal bandwidth. Our approach based on f_{IM} allows simultaneous tuning of the spacing between each mode pair. With a f_{IM} range of 12.5 GHz, our electronic synthesizer is able to seamlessly cover the whole mmW band and higher frequencies (Supplementary Section 7).

Phase stabilizing $\Delta\nu_{\mathrm{rep}}$ is the essential aspect of our electronic synthesizer. The key advantage is that the mmW frequency noise depends on $\Delta\nu_{\mathrm{rep}}$ rather than on the repetition rate of each soliton

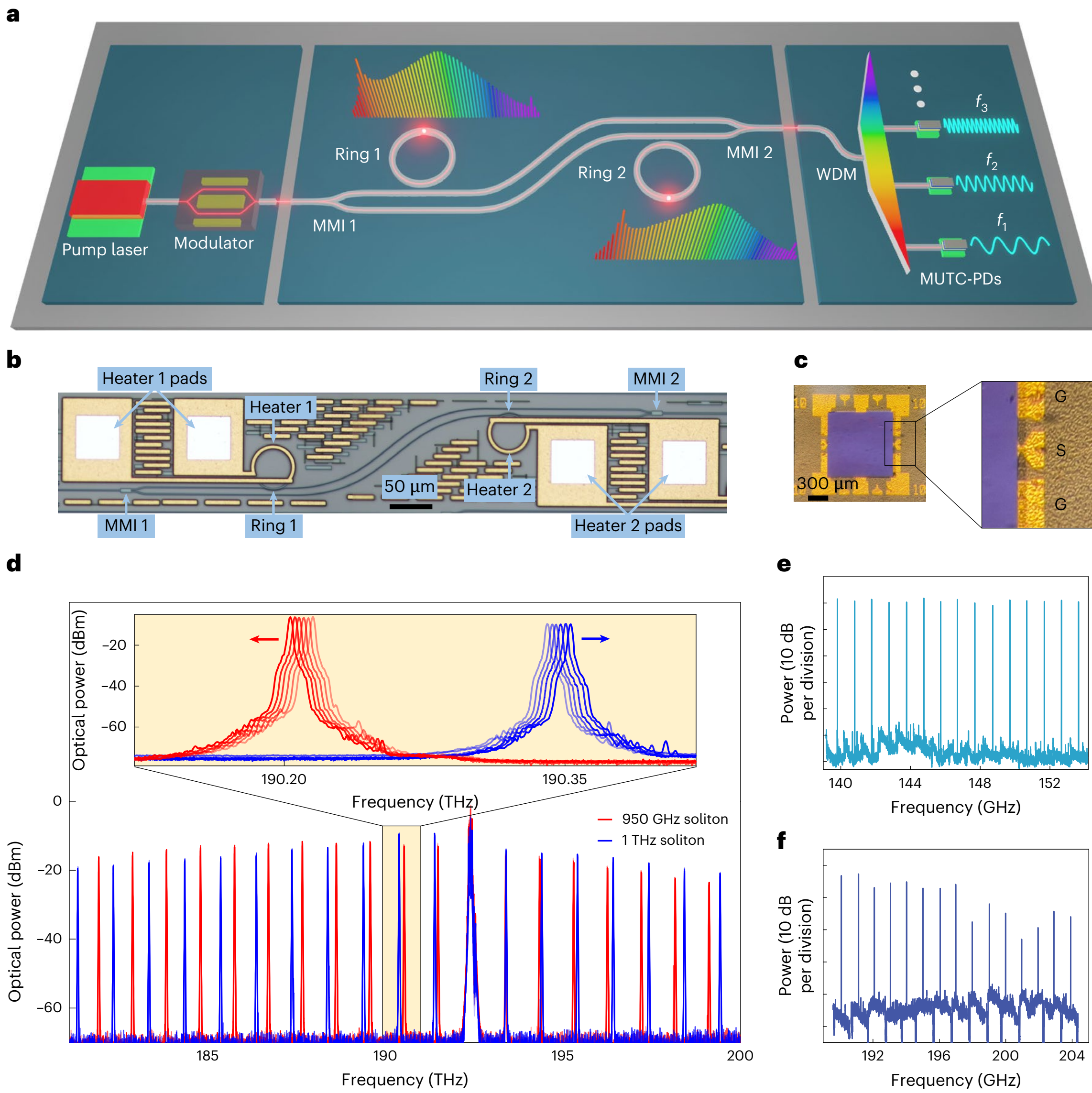

Fig. 1 | A wide-band mmW frequency synthesizer architecture using soliton microcomb photomixing. a, Conceptual diagram of the chip-scale mmW synthesizer. MUTC-PD, MUTC photodiode. **b**, Integrated soliton dual-comb generator. **c**, Microscope image of the high-speed MUTC photodiode, which is flip-chip bonded on the aluminium nitride submount with a ground–signal–ground (GSG) coplanar waveguide. **d**, Comb spectra of f_{IM} tuning; for example, the inset shows an enlarged view of the mode pairs with ~150 GHz spacing. **e**,**f**, Electrical spectra of the 150 GHz (**e**) and 200 GHz (**f**) beat notes with a frequency tuning step size of 1 GHz.

microcomb; therefore, a fully stabilized microcomb is not required. We leverage the common-mode pump laser and near-perfect equidistance of the separate microcombs to transfer the stability of a low-frequency microwave clock (f_{clk}) directly to the mmW and THz ranges. The synthesizer output comes directly from $\Delta\nu_{rep}$ and f_{IM}. In particular, the spectra of the two microcombs are

$$\nu_{N1} = \nu_{p1} + N\nu_{rep1} \quad (1)$$

and

$$\nu_{N2} = \nu_{p2} + N\nu_{rep2}, \quad (2)$$

where ν_N, ν_p and ν_{rep} are the comb line frequencies, the pump frequencies and the repetition frequencies, respectively. The integer N is the comb mode index with respect to the pump, and it is negative (positive) for the comb modes at lower (higher) frequency with respect to the pump. Indeed, the optical heterodyne of commensurate mode numbers from each comb yields the fundamental output of our electronic synthesizer, namely

$$f_N = |\nu_{N1} - \nu_{N2}| = |2f_{IM} - N\Delta\nu_{rep}|, \quad (3)$$

where $2f_{IM} = \nu_{p1} - \nu_{p2}$ and f_{IM} is derived from f_{clk}, namely $f_{IM} = \alpha f_{clk}$, where α is a frequency multiplication factor. Equation (3) indicates that we can finely tune f_N by varying f_{IM} and coarsely change the frequency band of f_N by varying N, which is achieved by using a WDM filter or an OBPF to select different mode pairs for photodetection.

Figure 2 presents an overview of the phase-locking system and the fundamental phase-noise performance of the synthesizer, including a system diagram (Fig. 2a), an optical spectrum showing mode pairs for locking $\Delta\nu_{rep}$ (f_1) as well as mmW generation at f_N (Fig. 2b), and single-sideband (SSB) phase-noise measurements (Fig. 2c). As shown in Fig. 2a, the pump laser is modulated by an intensity modulator, generating two sidebands that serve as the pumps for two SiN microresonators with a free spectral range of 950 GHz and 1 THz, respectively

https://doi.org/10.1038/s41566-026-01898-z

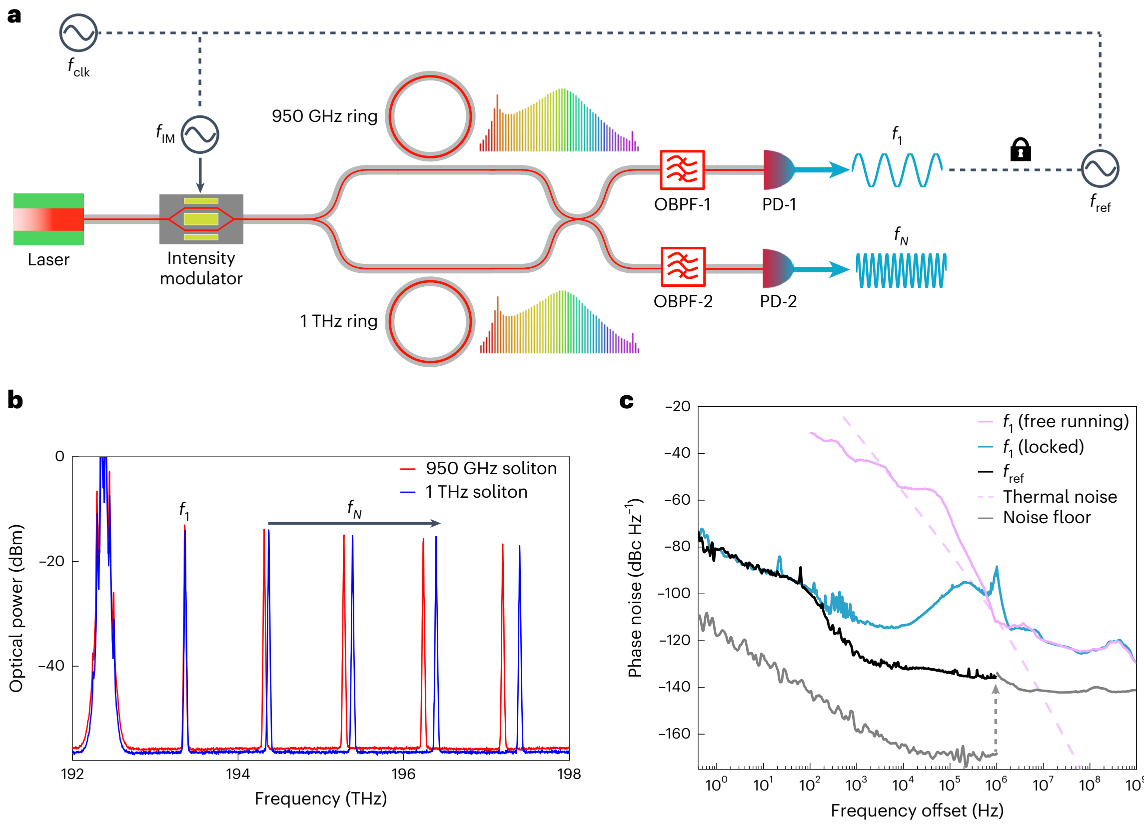

Fig. 2 | mmW frequency synthesis by locking f_1 to a stable reference clock f_{ref}. a, Experimental set-up, including a continuous-wave (CW) laser, an intensity modulator driven by f_{IM}, two microresonators on separated chips, two OBPFs, a low-speed photodiode (PD-1) to detect f_1 and a high-speed MUTC photodiode (PD-2) to detect f_N. **b**, Optical spectrum of the dual-soliton combs, emphasizing the first mode pair (f_1) for locking $\Delta\nu_{rep}$ and high-order mode pairs (f_N, $N > 1$) for mmW generation. **c**, A comparison of f_1 phase noise between the free-running (solid pink trace) and phase-locked (blue trace) cases. For reference, we also present the phase noise of f_{ref} (black trace), predicted thermal noise (dashed pink trace) and the noise floor of our phase-noise analyser (grey trace).

(Supplementary Sections 3 and 5). We initiate solitons in both microresonators simultaneously by fast sweeping the pump frequency across each resonance[43] (Methods; Supplementary Section 6). The two soliton microcombs are combined by a fibre coupler, followed by two tunable OBPFs to select different mode pairs for photodetection in a low-speed photodiode (PD-1) and a high-speed MUTC photodiode (PD-2), respectively.

To synthesize the mmW output f_N, we detect and lock the microcomb mode pair that corresponds to $f_1 = 2f_{IM} - \Delta\nu_{rep}$ ($2f_{IM} > \Delta\nu_{rep}$ in our experiment). By applying electronic feedback to the pump frequencies (Methods), we lock f_1 with a low-frequency reference f_{ref} that is synthesized to f_{clk}, namely $f_1 = f_{ref} = \beta f_{clk}$. Then, $\Delta\nu_{rep}$ is expressed as

$$\Delta\nu_{rep} = 2f_{IM} - f_1 = (2\alpha - \beta) f_{clk}. \quad (4)$$

Substituting equation (4) into equation (3), we can derive the expression for f_N as a function of f_{clk}:

$$f_N = |2\alpha(1 - N) + \beta N| f_{clk}, \quad (5)$$

where α, β and N are integers. Equation (5) shows that f_N is a phase-coherent multiplication of f_{clk}. After photodetection in the high-speed MUTC photodiode, we achieve precise frequency synthesis between a high-frequency f_N and the low-frequency f_{clk}, with user-defined integer ratios (α, β) and mode index (N).

Phase-noise analysis reveals that f_1 noise is mainly determined by f_{ref} noise, the PLL noise and the pump laser frequency noise. Figure 2c presents a comparison of the phase noise between the case with free-running (solid pink trace) and locked f_1 (blue trace). The noise floor of the phase-noise analyser is shown by the grey trace, with the discontinuity resulting from the use of different analysers below and above the 1-MHz frequency offset. For reference, we show the noise spectrum of f_{ref} at 100 MHz (black trace) and the predicted soliton microcomb thermal-noise contribution (dashed pink trace), respectively. Below 400-Hz frequency offset, the phase noise of f_1 is primarily determined by that of f_{ref}; from 400 Hz to 2 MHz, it is limited by the PLL noise; above 2 MHz, the frequency offset is beyond the PLL bandwidth, and the phase noise should follow the predicted thermal noise[43]. However, the noise level does not decrease sharply as we would expect based on microcomb thermal noise. Instead, there is a noise floor of −120 dBc Hz^{-1} at frequency offset above 1 MHz. We attribute this excess noise floor to the frequency noise of the pump laser. Equations (1) and (2) suggest that the pump frequency noise is transferred to each comb line directly or indirectly via the dependence of repetition frequency on detuning[43]. The 3-dB fibre couplers before and after the dual rings form an MZI structure. After passing through this fibre MZI and photodetection in PD-1, the pump frequency noise is further transferred to the beat note, resulting in the phase noise floor modified by the MZI transfer function (Supplementary Section 9).

Characterization of the synthesized mmW signals

Next, we investigate the phase-noise performance of f_N for $N = 3, 4, 5, 6$ and 7. The linewidth of the comb lines is primarily determined by that of the pump laser, which is below 200 kHz for the tunable laser we used (Velocity TLB-6700). The $1/f$ noise from the comb line pairs is greatly reduced within the bandwidth of the PLL. However, the $1/f$ noise from the low-frequency reference signal will be amplified through the frequency multiplexing process at higher frequencies. Because f_N is beyond the

 https://doi.org/10.1038/s41566-026-01898-z

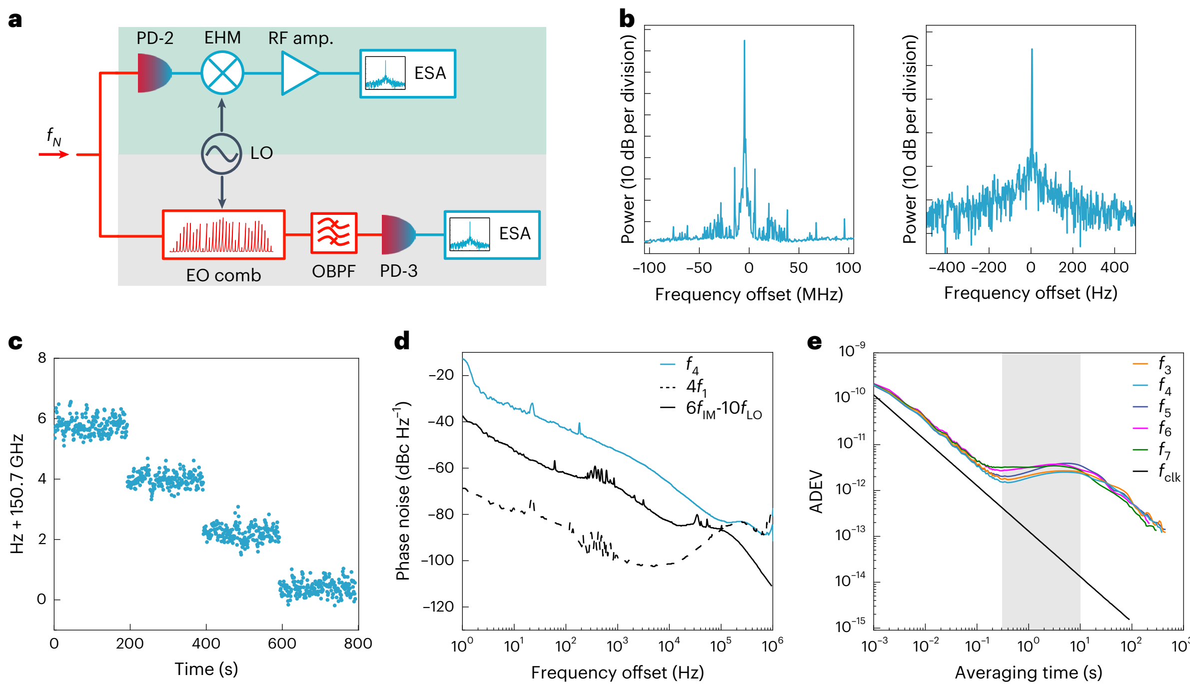

Fig. 3 | Characterization and fine frequency tuning of the synthesized mmW signals. a, Two methods of implementing frequency down-conversion: using an EHM (top) and EO combs (bottom). PD, photodetector; RF amp., RF amplifier. **b**, Electrical spectra of the 151-GHz mmW signal with a frequency span of 200 MHz (left) and 1 kHz (right), respectively. **c**, We finely tune the 150.7-GHz mmW signal with a step size of 1.8 Hz and wait for 200 s at each frequency. **d**, Measured phase noise of f_4 (blue trace). For comparison, we plot the phase noise contributed from the term $4f_1$ (dashed black trace) and the term $6f_{\mathrm{IM}} - 10f_{\mathrm{LO}}$ (solid black trace). **e**, Measured ADEV of f_{clk} (black) and f_N for $N = 3, 4, 5, 6$ and 7 (orange: $f_3 = 100$ GHz, light blue: $f_4 = 150$ GHz, violet-blue: $f_5 = 200$ GHz, magenta: $f_6 = 250$ GHz, green: $f_7 = 300$ GHz). The grey-shaded region indicates the ADEV floor of f_N.

operational bandwidth of our electrical spectrum analyser (ESA), we use two approaches for frequency downconversion to characterize f_N (Fig. 3a). In the first, we use a tunable 0.8-nm OBPF to select different mode pairs for photodetection. The beat notes at mmW frequencies are derived from the high-speed photodiode (PD-2) by a waveguide probe at 110 GHz to 170 GHz. An even harmonic mixer (EHM) working with a stable 15-GHz local oscillator (LO) downconverts the high-frequency beat notes to intermediate frequencies at ~100 MHz. In the second, the frequency downconversion is realized with two cascaded EO modulators[5]. Two comb modes are phase-modulated to generate sidebands that are spectrally overlapped. We use a narrow-band optical filter to select two sidebands that are close but derived from different comb lines, and detect f_{IF} with a low-speed photodiode (PD-3). In both cases, we convert f_N to an electrically detectable f_{IF} with the help of the stable f_{LO}, namely $f_{\mathrm{IF}} = f_N - Mf_{\mathrm{LO}}$, where M is a frequency multiplexing factor. Because we use a stable f_{LO} and its noise contribution is negligible, we can characterize f_N indirectly by measuring the low-frequency f_{IF}. Both methods characterize our mmW synthesizer output f_N of up to 300 GHz, and the results of the two approaches are in agreement.

Benefitting from the intrinsic low noise of the soliton microcombs, our electronic synthesizer generates mmW signals with a high signal-to-noise ratio. We experimentally generate up to 251-GHz mmW signal by photomixing mode pairs in the high-speed photodiode (Supplementary Section 8). This upper frequency limit is determined by the bandwidth of our MUTC photodiode and the measurement capability of our set-up, while the lower frequency limit extends down to d.c. For example, we present f_4 of 151 GHz in Fig. 3b, where the left and right panels show the electrical spectra with frequency span of 200 MHz and 1 kHz, respectively. The signal-to-noise ratio of 151-GHz mmW signal is 93 dB, with a few spurs in the electrical spectrum that are induced by the PLL and f_{ref}.

We demonstrate the frequency stability of our electronic synthesizer by its fine frequency tuning (Fig. 3c), phase noise (Fig. 3d) and Allan deviation (ADEV) (Fig. 3e) performance. Figure 3c depicts a linear frequency sweep of the mmW signal at 150 GHz (f_4), which is measured by a frequency counter with a gate time of 1 s after frequency downconversion. The step size of frequency sweep is 1.8 Hz, which is limited by the frequency stability of the generated mmW signal. We dwell for 200 s at each frequency to accumulate statistics on the synthesizer drift and fluctuation. The well-defined frequencies at such small tuning step, combined with the coarse tuning results in Fig. 1e, highlight the exceptional frequency tuning performance of our mmW synthesizer. Figure 3d shows the measured SSB phase noise of f_4 (blue trace), showing a phase noise of −83 dBc Hz^{-1} at 100-kHz offset. According to equation (4) and equation (3), f_{IF} can be expressed as $f_{\mathrm{IF}} = f_4 - 10f_{\mathrm{LO}} = 6f_{\mathrm{IM}} - 4f_1 - 10f_{\mathrm{LO}}$. For comparison, we plot the phase noise contributed from the term $6f_{\mathrm{IM}} - 10f_{\mathrm{LO}}$ (solid black trace) and the term $4f_1$ (dashed black trace), which are calculated by scaling the measured phase noise of f_{IM}, f_{LO} and f_1 by $20\log_{10}^{M}$, where M is the corresponding frequency multiplication factor. Below 30-kHz frequency offset, the phase noise of f_4 is ~20 dB higher than the predicted value, which we attribute to the noise induced by the 3-dB fibre coupler that combines the two soliton microcombs for photomixing[25]. Because the phase delay induced by the optical fibre is sensitive to ambient environmental factors, such as temperature and vibration, the phase difference of each mode pair fluctuates with time, leading to increased phase noise. This phase fluctuation also results as a floor in the measured ADEV traces[53] (Fig. 3e), where the ADEV floor is indicated by the grey-shaded region. Here, we use the EO modulation approach to characterize the ADEV of f_N. For comparison, the ADEV of f_{clk} is plotted as a black trace in Fig. 3e. Because of the phase-coherent frequency synthesis, the long-term ADEV of the mmW signal inherits the reference clock's stability and decreases with time. Despite the ADEV floor from 0.3 s to 10 s measurement times, the synthesizer output achieves a frequency instability below 3×10^{-12} at 1 s across the 100–300 GHz range. More photonic integration of the MMI couplers and both soliton microcombs

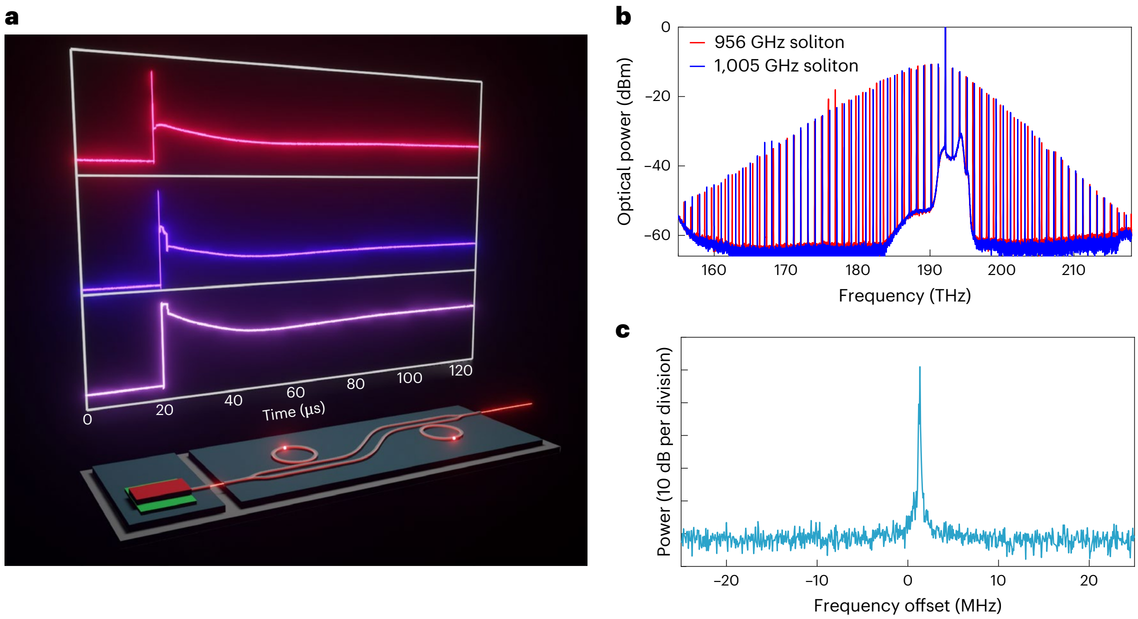

Fig. 4 | Soliton microcomb generation and photomixing using the integrated dual-comb generator. a, Oscilloscope traces of the comb power in the case with 956-GHz soliton only (top), 1,005-GHz soliton only (middle) and both simultaneously (bottom). **b**, Optical spectra of the two soliton microcombs with ν_{rep} of 956 GHz (red) and 1,005 GHz (blue). **c**, Electrical spectrum of the 147-GHz beat note corresponding to f_{-3}, which is measured with a resolution bandwidth of 30 kHz.

on one chip (Fig. 1b) will eliminate this ADEV floor and further improve the frequency stability.

Characterization of the integrated dual-comb generator

As a major step towards on-chip system integration, we create a dual-microcomb generator by integrating the 950-GHz and 1-THz rings, thermal heaters and MMI couplers on one chip. Figure 4a illustrates soliton generation with our integrated dual-microcomb, which is shown in the photograph of Fig. 1b. We tune the pump modes of the two resonators to the same frequency and use a continuous-wave laser as the pump for simplification. As with the bench-top system, we initiate the soliton by a fast pump-frequency sweep. After filtering out the pump, we monitor the comb power with a low-speed photodiode and an oscilloscope. The inset of Fig. 4a shows the oscilloscope traces as we initiate the solitons in a 956-GHz ring (top), a 1,005-GHz ring (middle) and both simultaneously (bottom). The corresponding microcomb optical spectra are shown in Fig. 4b, with blue and red traces representing the 1,005-GHz and 956-GHz soliton, respectively. For example, the comb line pairs corresponding to f_{-3} are selected by a tunable OBPF, followed by heterodyne detection with the high-speed MUTC photodiode. Figure 4c presents the beat note at 147 GHz after frequency downconversion to 946 MHz and spectral measurement with a resolution bandwidth of 30 kHz. After calibrating out the conversion loss of the EHM and the insertion loss of the waveguide probe, the RF power emitted by the MUTC photodiode is estimated to be −23 dBm. The successful generation of mmW signal demonstrates the potential of a fully integrated mmW frequency synthesizer.

Discussion

The key breakthrough of our chip-scale frequency synthesizer lies in its wide-band, precise and continuous frequency tuning capability (Supplementary Section 2), which is highly required in applications such as radar, imaging, high-precision spectroscopy and wireless communications. For example, the resolution of frequency-modulated continuous-wave radars is inversely proportional to the sweep bandwidth. A 300-GHz frequency sweep enables submillimetre range resolution, exceeding the performance of the current integrated frequency-modulated continuous-wave radars with a resolution of 1.97 mm (ref. 54). As another example, high-precision spectroscopy has been hindered by the lack of precisely tunable signal sources. Our d.c.–300 GHz continuously tunable synthesizer ensures broadband and seamless scanning of complex or unknown spectra. The 1.8-Hz frequency tuning step allows us to resolve extremely narrow spectroscopic lines, especially in gases and low-loss materials (typically in the kilohertz to megahertz range). Benefitting from its wide coverage, we can continuously characterize material responses from the microwave through the THz regime using a single measurement platform. Moreover, our design enables chip-scale integration, making it an extraordinary tool for future high-precision spectroscopy.

CMOS-based frequency synthesizers, which feature mature technology and low-power consumption, have superior performance at microwave frequencies, but their frequency tunability is limited to tens of gigahertz. By contrast, the proposed mmW frequency synthesizer offers broadband and continuous frequency tuning range from d.c. to THz. In the current implementation, it needs watt-level power input, which is much higher than that of CMOS-based ones. Future development of photonic technologies, such as microresonators with ultrahigh quality factors[55], low-bias, high-speed photodiodes[56], and high-efficiency microcombs[37], is expected to substantially reduce power consumption and increase the output power of the mmW signal.

In summary, we have introduced a wide-band mmW frequency synthesizer, based on dual microresonator-soliton photomixing. By pumping the two microresonators with a single intensity-modulated laser and locking the lowest-order mode pair of the dual microcomb, we generate exceptionally stable and tunable mmW signals, which are phase-coherently synthesized with respect to an input reference clock. We characterize the mmW synthesizer output over the range of d.c.–300 GHz and demonstrate an ADEV below 3×10^{-12} in 1-s measurements, limited by the reference clock and fibre delay noise in our set-up. Using a high-speed MUTC photodiode, we electrically generate a 150-GHz mmW signal with phase noise of −83 dBc Hz^{-1} at 100-kHz offset. The exceptional frequency tunability of our mmW synthesizer is highlighted by the coarse and fine tuning of 150 GHz mmW with a step size of 1 GHz and 1.8 Hz, respectively. Finally, we design a partially integrated version of our system and demonstrate 147-GHz mmW generation by photomixing mode pairs from the integrated dual-comb generator. Our work highlights an architecture for wide-band electronic synthesis, paving the way towards low-power, chip-scale mmW and THz frequency synthesizers with exceptional frequency stability and tunability.

Online content

Any methods, additional references, Nature Portfolio reporting summaries, source data, extended data, supplementary information, acknowledgements, peer review information; details of author contributions and competing interests; and statements of data and code availability are available at https://doi.org/10.1038/s41566-026-01898-z.

References

1. Jones, D. J. et al. Carrier-envelope phase control of femtosecond mode-locked lasers and direct optical frequency synthesis. *Science* **288**, 635–639 (2000).
2. Cundiff, S. T., Ye, J. & Hall, J. L. Optical frequency synthesis based on mode-locked lasers. *Rev. Sci. Instrum.* **72**, 3749–3771 (2001).
3. Fortier, T. M. et al. Generation of ultrastable microwaves via optical frequency division. *Nat. Photonics* **5**, 425–429 (2011).
4. Spencer, D. T. et al. An optical-frequency synthesizer using integrated photonics. *Nature* **557**, 81–85 (2018).
5. Drake, T. E. et al. Terahertz-rate Kerr-microresonator optical clockwork. *Phys. Rev. X* **9**, 031023 (2019).
6. Koenig, S. et al. Wireless sub-THz communication system with high data rate. *Nat. Photonics* **7**, 977–981 (2013).
7. Lien, J. et al. Soli: ubiquitous gesture sensing with millimeter wave radar. *ACM Trans. Graph.* **35**, 142 (2016).
8. Pauli, M. et al. Miniaturized millimeter-wave radar sensor for high-accuracy applications. *IEEE Trans. Microwave Theory Techn.* **65**, 1707–1715 (2017).
9. Beard, M. C., Turner, G. M. & Schmuttenmaer, C. A. Terahertz spectroscopy. *J. Phys. Chem. B* **106**, 7146–7159 (2002).
10. Jepsen, P., Cooke, D. & Koch, M. Terahertz spectroscopy and imaging – modern techniques and applications. *Laser Photonics Rev.* **5**, 124–166 (2011).
11. Booske, J. H. et al. Vacuum electronic high power terahertz sources. *IEEE Trans. Terahertz Sci. Technol.* **1**, 54–75 (2011).
12. Midford, T. A. & Bernick, R. L. Millimeter-wave CW impatt diodes and oscillators. *IEEE Trans. Microwave Theory Techn.* **27**, 483–492 (1979).
13. Eisele, H. & Kamoua, R. Submillimeter-wave InP Gunn devices. *IEEE Trans. Microwave Theory Techn.* **52**, 2371–2378 (2004).
14. Faist, J. et al. Quantum cascade laser. *Science* **264**, 553–556 (1994).
15. Wang, C.-C., Chen, Z. & Heydari, P. W-band silicon-based frequency synthesizers using injection-locked and harmonic triplers. *IEEE Trans. Microwave Theory Techn.* **60**, 1307–1320 (2012).
16. Musa, A. et al. A low phase noise quadrature injection locked frequency synthesizer for mm-wave applications. *IEEE J. Solid-State Circuits* **46**, 2635–2649 (2011).
17. Luo, T.-N., Wu, C.-H. E. & Chen, Y.-J. E. A 77-GHz CMOS FMCW frequency synthesizer with reconfigurable chirps. *IEEE Trans. Microwave Theory Techn.* **61**, 2641–2647 (2013).
18. Kim, J. et al. An ultra-low-jitter, mmW-band frequency synthesizer based on digital subsampling PLL using optimally spaced voltage comparators. *IEEE J. Solid-State Circuits* **54**, 3466–3477 (2019).
19. Meng, X., Chi, B., Liu, Y., Ma, T. & Wang, Z. A fully integrated 150-GHz transceiver front-end in 65-nm CMOS. *IEEE Trans. Circuits Systems II: Express Briefs* **66**, 602–606 (2019).
20. Lin, C.-T. et al. A continuously tunable and filterless optical millimeter-wave generation via frequency octupling. *Opt. Express* **17**, 19749–19756 (2009).
21. Fukushima, S., Silva, C., Muramoto, Y. & Seeds, A. Optoelectronic millimeter-wave synthesis using an optical frequency comb generator, optically injection locked lasers, and a unitraveling-carrier photodiode. *J. Lightwave Technol.* **21**, 3043–3051 (2003).
22. Musha, M. et al. A highly stable mm-wave synthesizer realized by mixing two lasers locked to an optical frequency comb generator. *Optics Commun.* **240**, 201–208 (2004).
23. Li, J., Lee, H. & Vahala, K. J. Microwave synthesizer using an on-chip Brillouin oscillator. *Nat. Commun.* **4**, 2097 (2013).
24. Li, Y. et al. Low-noise millimeter-wave synthesis from a dual-wavelength fiber Brillouin cavity. *Optics Lett.* **44**, 359–362 (2019).
25. Schneider, G. J., Murakowski, J. A., Schuetz, C. A., Shi, S. & Prather, D. W. Radiofrequency signal-generation system with over seven octaves of continuous tuning. *Nat. Photonics* **7**, 118–122 (2013).
26. Herr, T. et al. Temporal solitons in optical microresonators. *Nat. Photonics* **8**, 145–152 (2014).
27. Yi, X., Yang, Q.-F., Yang, K. Y., Suh, M.-G. & Vahala, K. Soliton frequency comb at microwave rates in a high-Q silica microresonator.*Optica* **2**, 1078–1085 (2015).
28. Xue, X. et al. Mode-locked dark pulse Kerr combs in normal-dispersion microresonators. *Nat. Photonics* **9**, 594–600 (2015).
29. Kippenberg, T. J., Gaeta, A. L., Lipson, M. & Gorodetsky, M. L. Dissipative Kerr solitons in optical microresonators. *Science* **361**, eaan8083 (2018).
30. Yu, S.-P. et al. Spontaneous pulse formation in edgeless photonic crystal resonators. *Nat. Photonics* **15**, 461–467 (2021).
31. Sun, Y. et al. Applications of optical microcombs. *Adv. Opt. Photon.* **15**, 86–175 (2023).
32. Liu, J. et al. Photonic microwave generation in the X- and K-band using integrated soliton microcombs. *Nat. Photonics* **14**, 486–491 (2020).
33. Wang, B. et al. Towards high-power, high-coherence, integrated photonic mmwave platform with microcavity solitons. *Light Sci. Appl.* **10**, 4 (2021).
34. Sun, W. et al. A chip-integrated comb-based microwave oscillator. *Light Sci. Appl.* **14**, 179 (2025).
35. Helgason, Ó. B. et al. Surpassing the nonlinear conversion efficiency of soliton microcombs. *Nat. Photonics* **17**, 992–999 (2023).
36. Yang, Q.-F., Hu, Y., Torres-Company, V. & Vahala, K. Efficient microresonator frequency combs. *eLight* **4**, 18 (2024).
37. Zang, J. et al. Laser power consumption of soliton formation in a bidirectional Kerr resonator. *Nat. Photonics* **19**, 510–517 (2025).
38. Papp, S. B. et al. Microresonator frequency comb optical clock. *Optica* **1**, 10–14 (2014).
39. Newman, Z. L. et al. Architecture for the photonic integration of an optical atomic clock. *Optica* **6**, 680–685 (2019).
40. Lucas, E. et al. Ultralow-noise photonic microwave synthesis using a soliton microcomb-based transfer oscillator. *Nat. Commun.* **11**, 374 (2020).
41. Kudelin, I. et al. Photonic chip-based low-noise microwave oscillator. *Nature* **627**, 534–539 (2024).
42. Sun, S. et al. Integrated optical frequency division for microwave and mmwave generation. *Nature* **627**, 540–545 (2024).
43. Stone, J. R. et al. Thermal and nonlinear dissipative-soliton dynamics in Kerr-microresonator frequency combs. *Phys. Rev. Lett.* **121**, 063902 (2018).
44. Nikpaik, A., Masnadi Shirazi, A. H., Nabavi, A., Mirabbasi, S. & Shekhar, S. A 219-to-231 GHz frequency-multiplier-based VCO with ~3% peak DC-to-RF efficiency in 65-nm CMOS. *IEEE J. Solid-State Circuits* **53**, 389–403 (2018).
45. Peng, Z. et al. A 300 GHz push–push coupling VCO employing t-embedded network in CMOS technology. *IEEE Trans. Terahertz Sci. Technol.* **12**, 426–429 (2022).

46. Dossanov, A., Lammert, V., Aichner, M. & Issakov, V. A 60 GHz frequency synthesizer in 0.13 μm SiGe BiCMOS for biomedical implant applications. In *2025 IEEE International Symposium on Circuits and Systems* 1–5 (IEEE, 2025).
47. Zang, J., Liu, H., Briles, T. C. & Papp, S. B. Foundry manufacturing of octave-spanning microcombs. *Opt. Lett.* **49**, 5143–5146 (2024).
48. Li, Q. et al. High-power flip-chip bonded photodiode with 110 GHz bandwidth. *J. Lightwave Technol.* **34**, 2139–2144 (2016).
49. Morgan, J. S. et al. High-power flip-chip bonded modified uni-traveling carrier photodiodes with −2.6 dbm RF output power at 160 GHz. In 2018 *IEEE Photonics Conference* 1–2 (IEEE, 2018).
50. Zang, J., Morgan, J. S., Beling, A. & Papp, S. B. Broadband optoelectronic mixer for terahertz frequency-comb measurements. *Opt. Lett.* **50**, 3173–3176 (2025).
51. Dai, D. et al. Low-loss Si_3N_4 arrayed-waveguide grating (de) multiplexer using nano-core optical waveguides. *Opt. Express* **19**, 14130–14136 (2011).
52. Pirmoradi, A. et al. Integrated multi-port multi-wavelength coherent optical source for beyond Tb/s optical links. *Nat. Commun.* **16**, 6387 (2025).
53. Wu, K. et al. Vernier microcombs for integrated optical atomic clocks. *Nat. Photonics* **19**, 400–406 (2025).
54. Ziegler-Bellenberg, T. et al. A high-resolution 300-GHz FMCW-radar sensor using a dual-function SiGe transceiver MMIC. *Int. J. Microwave Wireless Technol.* **17**, 1603–1615 (2025).
55. Liu, J. et al. Ultralow-power chip-based soliton microcombs for photonic integration. *Optica* **5**, 1347–1353 (2018).
56. Morgan, J. S. et al. Bias-insensitive GaAsSb/InP CC-MUTC photodiodes for mmwave generation up to 325 GHz. *J. Lightwave Technol.* **41**, 7092–7097 (2023).

Methods

High-speed photodiode design

The MUTC photodiode is specifically designed for high-frequency, high-power operation by allowing only fast electron transitions through the depleted region. The overall photodiode bandwidth depends on the transit time and *RC*-limited bandwidth. The former refers to the time delay between carrier generation in the absorption layers and carrier collection in the contacts, while the latter is mainly induced by the photodiode's series resistance and junction capacitance. We use an absorption layer of 150 nm and drift layer of 350 nm to reduce the transit time-limited bandwidth, and the photodiode diameter is 5 µm, reducing the junction capacitance for large *RC*-limited bandwidth. The photodiode is flip-chip bonded to an aluminium-nitride submount to efficiently remove heat and simplify mmW measurement with a ground–signal–ground probe. The coplanar waveguide on the submount is optimized to extend the overall bandwidth by inductive peaking.

Soliton generation and f_1 locking

The comb formation process in microresonators include several comb states, which highly depends on the pump-resonance detuning, pump power and cavity dispersion. We access the stable soliton states using a rapid frequency sweeping technique. First we optimize the laser frequency and f_{IM} to align two modulation sidebands with two microresonators' resonances. Then, the two sidebands are coupled into a dual parallel Mach–Zehnder modulator whose modulation signal is derived from a VCO. We operate the dual parallel Mach–Zehnder modulator at SSB suppressed-carrier modulation (SSB-SC) mode to induce a common pump frequency shift for both microresonators. This pump frequency shift is determined by the VCO and varies with the VCO's bias voltage (tuning rate ~1 GHz V^{-1}). By applying an appropriate ramp signal to the VCO, we are able to fast sweep (>100 GHz μs^{-1}) the pump frequency and simultaneously excite solitons in both microresonators.

To lock f_1, we use a voltage adder at the input of VCO. The control signal applied to the VCO is formed by combining two inputs: one is the above-mentioned ramp signal for soliton generation; another is the electronic feedback signal from the phase lock servo. This feedback signal is properly attenuated and induces a small but common change of the pump-cavity detuning in both microresonators. The dependence of soliton repetition rates on detuning is different in 950-GHz and 1-THz microresonators; therefore, $\Delta\nu_{rep}$ varies with detuning. Because $f_1 = |2f_{IM} - \Delta\nu_{rep}|$ and f_{IM} remains fixed during the locking process, f_1 also varies with detuning and can be finely tuned by the feedback signal.

Coarse frequency tuning of the mmW synthesizer

Wide-band mmW frequency tuning is realized by f_{IM} tuning, which equivalently varies the pump frequencies because the laser frequency is fixed. During this process, maintaining the soliton state in both microresonators is challenging, as it exists only within a specific detuning range. Because the resonant frequency highly depends on the device temperature, we develop a computer-controlled lookup-table method to thermally tune the resonant frequency so that it can track the pump frequency automatically and keep the detuning in the soliton existence range. In Fig. 1e,f, we maintain the soliton state in both microresonators over the entire 13-GHz tuning range, which is limited by the operating bandwidth of the RF amplifier used for intensity modulation.

Data availability

The data supporting the findings of this study are available via figshare at https://doi.org/10.6084/m9.figshare.31736749 (ref. 57).

Code availability

The codes that support the findings of this study are available from the corresponding authors upon reasonable request.

References

57. Zang, J., Briles, T. C., Morgan, J. S., Beling, A. & Papp, S. B. Raw data for 'wide-band millimeter-wave synthesizer using microresonator-soliton photomixing'. *figshare* https://doi.org/10.6084/m9.figshare.31736749 (2026).

Acknowledgements

We acknowledge M. Woodson and S. Estrella from Freedom Photonics for MUTC PD fabrication. We thank A. Carollo and H. Liu for technical review of the letter. This research has been funded by the AFOSR FA9550-20-1-0004 project number 19RT1019 (S.B.P.), DARPA DODOS (J.Z., T.C.B., J.S.M., A.B. and S.B.P.), NSF Quantum Leap Challenge Institute Award OMA-2016244 (S.B.P.) and NIST (S.B.P.). This work is a contribution of the US government and is not subject to copyright. Trade names provide information only and not an endorsement.

Author contributions

J.Z. and S.B.P. conceived the experiment. J.Z. and T.C.B. performed the system measurements. J.S.M. designed and characterized the high-speed MUTC photodiode. J.Z. designed and tested the integrated dual-comb generator. J.Z. and S.B.P analysed the experimental results and wrote the paper. S.B.P. and A.B. supervised the project. All authors discussed the results and contributed to the final manuscript.

Competing interests

S.B.P. and J.Z have filed a US patent (US11336377B1) regarding the technology reported in this article. The other authors declare no competing interests.

Additional information

Supplementary information The online version contains supplementary material available at https://doi.org/10.1038/s41566-026-01898-z.

Correspondence and requests for materials should be addressed to Jizhao Zang or Scott B. Papp.

Peer review information *Nature Photonics* thanks the anonymous reviewers for their contribution to the peer review of this work. Peer reviewer reports are available.